Journal of Solid State Chemistry 183 (2010) 2466–2474

Contents lists available at ScienceDirect

Journal of Solid State Chemistry

journal homepage: www.elsevier.com/locate/jssc

Microwave hydrothermal synthesis and photocatalytic activity of $AgIn_5S_8$ for the degradation of dye

Wenjuan Zhang, Danzhen Li*, Meng Sun, Yu Shao, Zhixin Chen, Guangcan Xiao, Xianzhi Fu

Research Institute of Photocatalysis, State Key Laboratory Breeding Base of Photocatalysis, Fuzhou University, Fuzhou, Fujian 350002, PR China

ARTICLE INFO

Article history:
Received 28 May 2010
Received in revised form
6 August 2010
Accepted 9 August 2010
Available online 12 August 2010

Keywords:
Photocatalyst
$AgIn_5S_8$
Microwave hydrothermal
Visible light
Methyl orange

ABSTRACT

$AgIn_5S_8$ powders were successfully synthesized by a microwave hydrothermal method for the first time. This method is a mild and highly efficient route involves no templates, catalysts, or surfactants. Therefore, it is very promising for the low-cost and large-scale industrial production. The samples were characterized by X-ray diffraction, UV–vis spectroscopy, X-ray photoelectron spectroscopy, and scanning electron microscopy. The photocatalytic activity of $AgIn_5S_8$ nanoparticles was investigated through the degradation of methyl orange under visible light irradiation. Compared with $TiO_{2-x}N_x$, $AgIn_5S_8$ has exhibited a superior activity under the same condition. A liquid chromatogram-mass spectrometer was used to separate and identify the dye and degradation products generated during the reaction. According to the experiment results, a possible mechanism for the degradation of organic pollutant over $AgIn_5S_8$ was proposed.

1. Introduction

A large number of industrial toxic pollutants are often discharged into rivers. The pollutants are difficult to decompose by natural means and very hazardous to human health [1]. During the past two decades, photocatalytic technology involving TiO_2 semiconductor particles has been successfully applied in decomposition of a wide range of toxic organic pollutants in wastewater or air [2,3]. However, TiO_2 can only be activated by ultraviolet (UV) light because of the wide band gap of 3.2 eV (anatase) [4]. Artificial UV light sources tend to be somewhat expensive, and the UV light reaching the surface of the earth and available to excite TiO_2 is relatively small (ca. 3–5% of the AM1 solar spectrum) [5]. Therefore, to exploit visible light active photocatalysts with high quantum efficiency and high stability is significant in the development of photocatalysis.

Recently, semiconductor materials of ternary chalcogenide compounds XY_mZ_n (X=Ag, Zn, Cd, etc.; Y=Al, Ga, In; Z=S, Se, Te; m, n=integer) have been studied in the optoelectronic and photocatalytic field [6–10], and some of them were effective in photocatalysis [9,10]. As one of the ternary chalcogenide compounds, $AgIn_5S_8$ has been reported to be favorable for the application in the photovoltaic and photochemical field [11]. Konovalov et al. [11] found that CuI/$AgIn_5S_8$ heterojunction might be applied in photovoltaic devices. According to their report, n-type $AgIn_5S_8$ was an attractive candidate for absorber layers of top cells in 4-terminal tandem structures. Chen and Ye [9] reported that $AgIn_5S_8$ showed high photocatalytic activity for the evolution of hydrogen under visible light irradiation. So, it is attractive to know whether $AgIn_5S_8$ could decompose environmental pollutants under visible light irradiation.

There are many methods reported for the preparation of $AgIn_5S_8$, such as pulsed laser deposition approach [12], single crystal thermal evaporation [13], solution growth technique [14], and chemical bath deposition method [15]. However, all these methods have some limitation and disadvantage. (1) Some methods mentioned above involve at least two steps [9], indicating the synthesis process is sophisticated. (2) Until now researches mainly focus on the preparation of $AgIn_5S_8$ film, while the preparation of $AgIn_5S_8$ powder is rarely reported. (3) Many approaches are operated under harsh condition such as high temperature [12] or high vacuum [13]. (4) The $AgIn_5S_8$ samples which are synthesized with these methods usually are not pure phase [14]. (5) The preparation of $AgIn_5S_8$ through these methods usually costs a long time. Therefore, it is necessary to explore a simple, mild, and efficient method for the preparation of $AgIn_5S_8$ powder.

Herein, we successfully apply a microwave hydrothermal method to synthesize pure $AgIn_5S_8$ powder without any catalyst, template, or surfactant. This method has the advantage of simplicity, efficiency, time-saving, and safety. As we all know, microwave irradiation provides a rapid and homogeneous heating of the entire system, enhances reaction rates, and facilitates formation of uniform nucleation centers. It is energy efficient

* Corresponding author. Fax: +86 591 83779256.
E-mail address: dzli@fzu.edu.cn (D. Li).

0022-4596/$ - see front matter © 2010 Elsevier Inc. All rights reserved.
doi:10.1016/j.jssc.2010.08.011

and environment friendly [16]. So compared to other methods in photocatalyst synthesis, microwave heating techniques are potentially competitive for scale-up industrial production of high-quality photocatalysts. The as-synthesized sample has exhibited strong photocatalytic activity in the decomposition of methyl orange (MO) under visible light irradiation, compared with $TiO_{2-x}N_x$ photocatalyst. A liquid chromatography mass spectroscopy (LCMS) was applied for the identification of decomposed products, and a possible degradation path of MO by $AgIn_5S_8$ was proposed. The experiment for the detection of the active species was carried out. Through these experiments, the mechanism related to the photocatalytic process was proposed and discussed.

2. Experimental details

2.1. Synthesis

All reagents were analytical grade and used as received without further purification. In a typical procedure, 0.1 mmol Ag_2SO_4, 0.5 mmol $InCl_3 \cdot 4\ H_2O$, and an excess of thioacetamide were dissolved in 15 mL deionized water. Hydrochloric acid solution was added to adjust the pH value of the mixture to 4. Then, this solution was transferred into a glass vessel of 35 mL capacity and maintained at different temperatures (80, 120, 160, and 200 °C) for 10 min. The microwave hydrothermal synthesis was performed in a single mode CEM discovers system (Explorer 48, CEM Co.). When the reaction was completed, the reaction system was rapidly cooled using high pressure air (40 psi). The product was collected, and washed several times with deionized water and absolute ethanol. The final sample was dried at 80 °C for 12 h for characterization.

$TiO_{2-x}N_x$ product was also synthesized for the photocatalytic activity comparison. The amorphous TiO_2 xeogel was first prepared by a sol–gel method. The as-prepared TiO_2 xeogel was heated at 400 °C for 3 h under flowing NH_3 gas, and then annealed at 400 °C for 2 h in static air to produce the final $TiO_{2-x}N_x$ sample [17].

2.2. Characterization

The X-ray diffraction (XRD) patterns were obtained by a Bruker D8 Advance X-ray diffractometer using Cu$K\alpha_1$ irradiation at 40 kV and 40 mA. Scanning electron microscopy (SEM) image was obtained on a JEOL JSM 6700F instrument operated at 20 kV and equipped with an energy-dispersive X-ray (EDX) analyzer (Phoenix). Transmission electron microscopy (TEM) and high-resolution TEM (HRTEM) were measured on a JEOL JEM 2010F microscope working at 200 kV. UV–vis diffuse reflectance spectra (DRS) were obtained by a Varian Cary 500 UV–vis–NIR spectrophotometer. The specific surface area was measured by N_2 adsorption at 77 K on a Micrometritics ASAP2020 analyzer. X-ray photoelectron spectroscopy (XPS) analysis was conducted on an ESCALAB 250 photoelectron spectroscope (Thermo Fisher Scientific) at 3.0×10^{-10} mbar with monochromatic Al$K\alpha$ radiation. A conventional three electrode cells using a PAR VMP3 Multi Potentiotat apparatus was used to determine the flatband potential (V_{fb}). The catalyst sample was deposited on a 1 cm × 1 cm ITO conducting glass served as working electrode, while the saturated calomel electrode (SCE) as the reference electrode and Pt as the counter electrode. The Mott–Schottky plot to evaluate the V_{fb} of the semiconductor space charge region was obtained by measuring impedance spectra at fixed frequency of 1 kHz. The electron spin resonance (ESR) signals of the radicals spin-trapped by 5,5-dimethyl-*l*-pyrroline-*N*-oxide (DMPO) were recorded with a Bruker EMX A300 spectrometer after irradiation of methanol or aqueous dispersions. The irradiation source was a 500 W Xe-arc lamp equipped with an IR-cutoff filter and a UV-cutoff filter. Hydrogen peroxide (H_2O_2) was determined by a photometric method in which *N*,*N*-diethyl-*p*-phenylenediamine (DPD) is oxidized by a peroxidase (POD) catalyzed reaction. After 30 min of visible light irradiation, the $AgIn_5S_8/H_2O$ (40 mg/80 mL) suspension was immediately centrifuged to remove the catalysts and analyzed to detect the formation of H_2O_2. The procedure of DPD method was according to the literature [18].

2.3. LCMS analysis

The LCMS system was equipped with a Zorbax C_{18} column (150 mm length × 4.6 mm i.d., 5 μm), and coupled online to an LC/MSD Trap XCT ion-trap mass spectrometer (Agilent Technologies, CA, USA). The mass spectrometer (MS) was equipped with an electrospray ionization (ESI) source and operated in positive polarity. The solvents used as mobile phase were acetonitrile: 0.01 M ammonium acetate (pH 6.8)=30:70 (V/V), flow rate was 0.6 mL min^{-1}, 20 μL of standard or sample solution was injected, and the mass range was from 50 to 600 *m*/*z*.

2.4. Photocatalytic activity measurements

The photocatalytic degradations of MO were conducted in an aqueous solution under visible light irradiation. 40 mg of $AgIn_5S_8$ was added into 80 mL of MO solution (10 mg L^{-1}). The visible light source was a 500 W tungsten–halogen lamp (Philips Electronics), and a fan and circulating water were used to avoid overheating. Two cutoff filters were equipped to restrict the illumination only in the range of 420–800 nm. Before irradiation, the suspension was stirred for 1 h in dark to ensure the establishment of adsorption–desorption equilibrium. 3 mL of aliquots were sampled at a given time during the photocatalytic progress, which were then centrifuged to remove the catalysts. A Varian Cary 50 Scan UV–vis spectrophotometer was used to monitor the concentration changes of MO. After the photocatalytic reaction, the photocatalysts were collected and washed for further characterization. The percentage of degradation is evaluated by C/C_0. C is the maximum intensity of MO absorption spectra for each irradiated time interval at a wavelength 464 nm, and C_0 is the absorption intensity of the initial MO concentration when adsorption–desorption equilibrium was achieved. The total organic carbon (TOC) values were detected by a Shimadzu TOC-V_{CPH} total organic carbon analyzer. The experiment details of TOC were the same with the photocatalytic activity experiment.

3. Results and discussion

3.1. XRD

Fig. 1 showed the XRD patterns of the $AgIn_5S_8$ samples prepared at different temperatures (80, 120, 160, and 200 °C). As we can see, the XRD patterns of the samples prepared at different temperatures are nearly in the same position. And all the diffraction peaks could be indexed to a pure cubic phase of $AgIn_5S_8$ (JCPDS no. 26-1477), which was in agreement with the literatures [9,19]. No peaks of impurities have been observed in XRD figures. However, the diffraction peaks of the sample prepared at 80 °C was rather weak compared with that of other samples, indicating the imperfect crystallization occurred at low temperature. This result indicated that $AgIn_5S_8$ could be easily

synthesized under the current synthetic conditions. The average crystallite size of the $AgIn_5S_8$ sample prepared at 120 °C was calculated by the Scherrer formula. The average crystallite size for this sample was around 29.6 nm. In addition, the sample prepared at 120 °C displayed the best photocatalytic activity as show in Fig. 5(a). So in this work, the study was focused on the sample prepared at 120 °C.

3.2. Morphology of $AgIn_5S_8$ crystalline

The SEM technology was used to detect the overall morphology of the as-prepared $AgIn_5S_8$. A typical SEM micrograph (Fig. 2a) showed that the as-prepared $AgIn_5S_8$ was composed of a large quantity of nanoparticles with relative uniform grain size. The TEM image shown in Fig. 2b further verified the morphology. The HRTEM image (Fig. 2c) showed that the fringes of $d=0.62$ nm matched the (111) crystallographic plane of the $AgIn_5S_8$ sample. The EDX pattern (Fig. 2d) recorded in SEM displayed the sample contained only Ag, In, and S elements. The molar ratio of Ag:In:S of as-prepared $AgIn_5S_8$ sample was 1:5.65:8.36, which was close to the stoichiometric composition. Therefore, the result of HRTEM and EDX measurements confirmed that the as-synthesized product was the pure $AgIn_5S_8$.

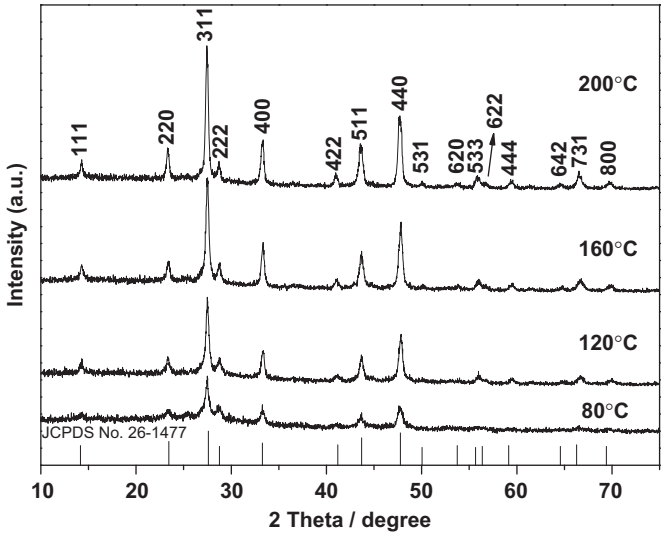

Fig. 1. XRD patterns of $AgIn_5S_8$ samples prepared at different temperatures.

3.3. DRS and BET

A diffuse reflectance spectrophotometer was applied to characterize the optical property of the as-prepared $AgIn_5S_8$. Fig. 3 showed the UV–vis diffuse reflectance spectrum of the $AgIn_5S_8$ powder. The spectrum had an absorption edge in the visible range, which indicated the absorption relevant to the band gap was due to the intrinsic transition of the material rather than the transition from impurity levels.

It is well known that the optical absorption near the band edge follows the equation: $\alpha h\nu = A(h\nu - E_g)^{n/2}$ (where α, $h\nu$, A, and E_g are absorption coefficient, incident photon energy, proportionality constant, and band gap, respectively, and the value of n depends on whether the transition is direct ($n=1$) or indirect ($n=4$)) [20,21]. According to the electronic structure calculation by density functional theory (DFT), $AgIn_5S_8$ is a direct gap semiconductor, as shown in Fig. S1 of Supplementary Material. As a result, for $AgIn_5S_8$, the relation between α, $h\nu$, and E_g can be described by the formula: $(\alpha h\nu)^2 = A(h\nu - E_g)$. From this equation, E_g could be obtained through extrapolating the linear relation to $(\alpha h\nu)^2 = 0$. So the E_g of $AgIn_5S_8$ sample was about 2.57 eV (inset of Fig. 3).

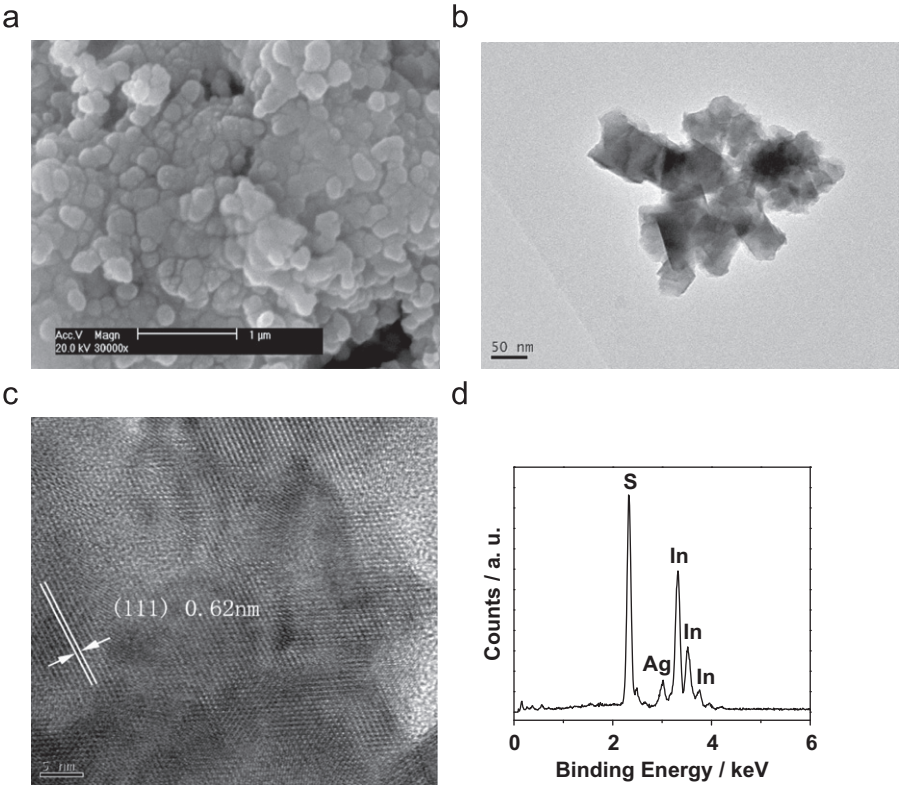

Fig. 2. SEM image (a), TEM image (b), high resolution TEM image (c), typical EDX pattern, and (d) of the as-prepared $AgIn_5S_8$ nanoparticles.

The nitrogen adsorption–desorption isotherms of the as-prepared $AgIn_5S_8$ sample were further investigated. The nitrogen adsorption isotherm for the as-synthesized $AgIn_5S_8$ (Fig. 4) is a type-IV isotherm, indicating the presence of mesoporous materials. The Brunquer–Emmett–Teller (BET) specific surface area of the $AgIn_5S_8$ sample prepared at 120 °C was 27.89 $m^2\,g^{-1}$.

3.4. Photocatalytic activity of $AgIn_5S_8$ catalyst

As shown in Fig. 5(a), the photocatalytic activity of $AgIn_5S_8$ prepared at different temperatures (80, 120, 160, and 200 °C) for decomposing MO was investigated under visible light. The result showed that the sample prepared at 120 °C displayed the best photocatalytic activity. The inset of Fig. 5(a) showed the absorption spectra of MO solution decomposed by the $AgIn_5S_8$ photocatalyst prepared at 120 °C under visible light irradiation. After 4 h of illumination time, the main absorption peak of MO (λ=464 nm) nearly disappeared (inset of Fig. 5(a)). In addition, $TiO_{2-x}N_x$ was used as a reference, because it has been studied a lot as visible light responsive photocatalyst [17,22]. The decomposition ratio of MO over $AgIn_5S_8$ prepared at 120 °C was about 89.4%, whereas that of $TiO_{2-x}N_x$ was only 8.9%. As shown in Fig. 5(b), two preliminary comparative experiments were carried out. It has revealed that MO could hardly be decomposed via $AgIn_5S_8$ in the dark, while in the blank experiment without $AgIn_5S_8$, the concentration of MO only slightly changed during 4 h of visible light irradiation. The result demonstrated $AgIn_5S_8$ exhibited a superior activity compared with $TiO_{2-x}N_x$ under the same condition.

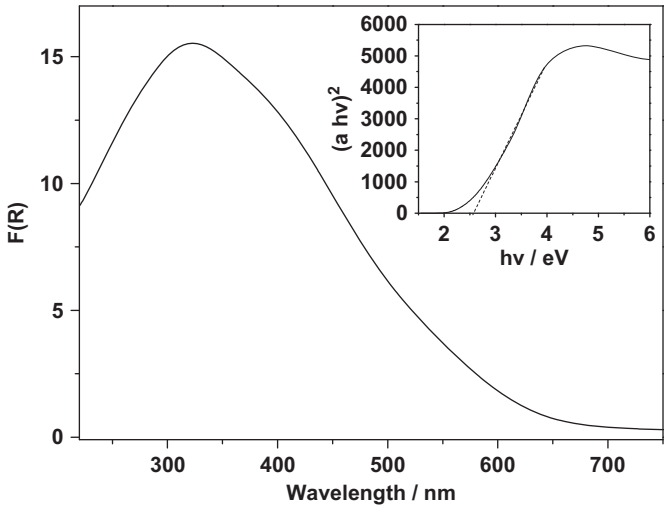

Fig. 3. Diffuse reflectance spectrum F(R) of the $AgIn_5S_8$ sample and the band gap energy E_g of $AgIn_5S_8$ (inset).

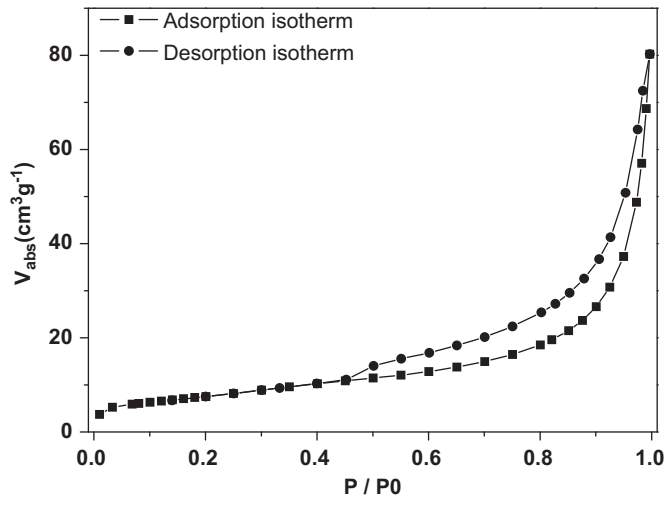

Fig. 4. Nitrogen adsorption–desorption isotherm plot for $AgIn_5S_8$ prepared at 120 °C.

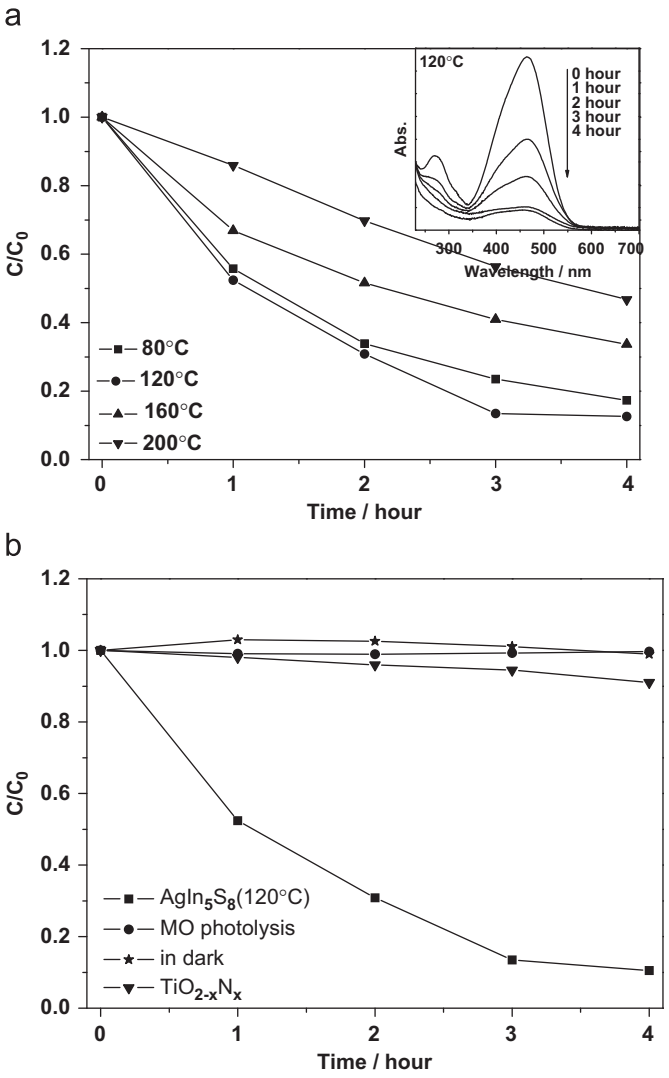

Fig. 5. Visible light photocatalytic activities of (a) $AgIn_5S_8$ products prepared at different temperatures and the insert showed the absorption spectra of MO solution decomposed by the $AgIn_5S_8$ photocatalyst prepared at 120 °C under visible light irradiation; (b) $AgIn_5S_8$ sample prepared at 120 °C and $TiO_{2-x}N_x$ by degrading MO.

3.5. LCMS and TOC

The decomposed products generated during the irradiation process were separated and identified by the LCMS technology. Fig. 6(T0–T4) showed the chromatograms of the MO solution sampled at different irradiation intervals. As we can see, only one peak (7.4 min) which belonged to MO was observed in the chromatogram of 0 h (before irradiation). During the 4 h of visible light irradiation time, the intensity of MO peak (7.4 min) decreased gradually (Fig. 6). After the initial 1 h of irradiation (Fig. 6—T1), two new peaks belonging to the byproducts appeared at 4.2 and 2.2 min in the chromatogram of 1 h. The intensity of the peak appeared at 4.2 min rose in the initial 2 h, and then had

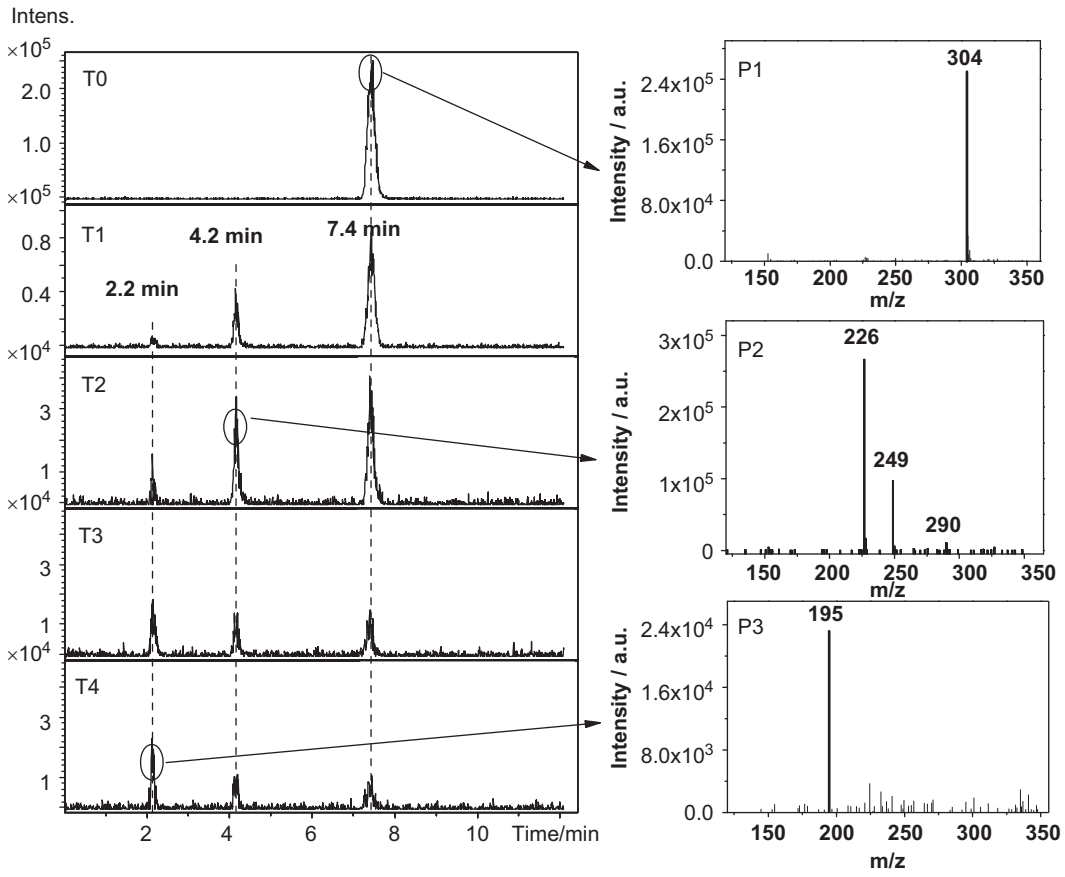

Fig. 6. LCMS chromatograms of the MO solutions at different irradiation intervals: (T0) chromatogram of the original MO solution after adsorption–desorption equilibrium established without visible light irradiation; (T1)–(T4) chromatogram of the MO solution after 1, 2, 3, and 4 h of irradiation, respectively; (P1)–(P3) mass spectrum views of peak appeared at 7.4, 4.2, and 2.2 min according to the chromatograms.

a tendency to decrease; while that of the peak appear at 2.2 min increased gradually during 4 h of visible light illumination. These results suggested that some byproducts were first generated and their peaks appeared at 4.2 min in the chromatogram. These byproducts were subsequently degraded into other byproducts appearing at 2.2 min. However, after 4 h of reaction, the decomposed products and a small amount of MO were still present, indicating the incomplete degradation under this condition.

In order to reveal the structure of byproducts generated during the degradation process, the corresponding mass spectrum views of three peaks were collected. Figs. 6(P1), 6(P2), and 6(P3) showed the corresponding mass spectrum views of peaks appeared at 7.4, 4.2, and 2.2 min, respectively. In the mass spectrum of Fig. 6(P1), only one mass peak with $m/z=304$ was observed. It belonged to MO. As shown in Fig. 7, the intensity of MO peak continuously decreased with time. The mass spectrum of Figs. 6(P2) and 6(P3) showed that there were some byproducts with different m/z values (226, 249, 290, and 195) were generated. Mass spectra view changes of the peak intensity of the byproducts were shown in Fig. 7. The intensity of the mass peak with $m/z=290$ increased in the initial irradiation stage (1 h), but then decreased in the following 3 h. The intensity of the mass peak with $m/z=195$ increased gradually during the whole reaction process. So, we inferred the possible structures of the byproducts with $m/z=195$ and 290 and their possible degradation path (Scheme 1). During reaction, the demethylation of MO was carried out. One methyl group ($-CH_3$) bonded to the nitrogen atom in the MO molecule was removed, leading to the formation of the byproduct with m/z value of 290. Then, the demethylation of this byproduct continued

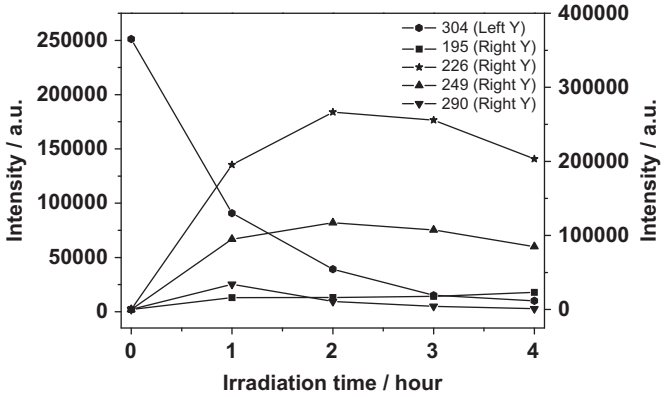

Fig. 7. Mass spectra view changes of the peak intensity appearing in the photocatalytic process of MO and the byproducts.

to carry out, accompanying with a desulfonation. This process finally lead to the formation of the byproduct with $m/z=195$. However, after N–C bond breaking, the p orbit of N atom participated in conjugation of the rest structure. As a result, the byproduct of $m/z=195$ is much more stable and it is difficult to be degraded. The intensity of the mass peak with $m/z=226$ and 249 both increased in the initial irradiation stage (2 h) but decreased a little when the irradiation time was prolonged to 4 h. The variation trend of these two mass peaks accorded with the chromatogram graphs (Fig. 6). It is worth to mention that opening ring was also observed during the photocatalytic process. Base on the experiment results and the discussion above, we inferred the

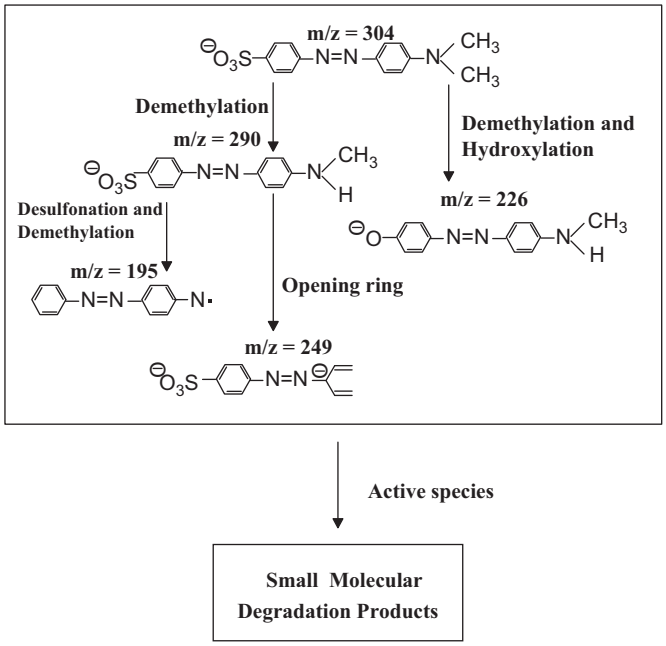

Scheme 1. Proposed degradation path for MO over $AgIn_5S_8$.

Table 1
TOC Result of MO during Photocatalytic Reaction.

Irradiation time	0 h	3 h	9 h	13 h	15 h
TOC (mg L^{-1})	4.683	4.178	3.391	2.662	2.550

possible structures of other decomposed byproducts and pathway of the photodegradation (Scheme 1).

The TOC of the bulk solution after removal of $AgIn_5S_8$ particles was also detected. Changes in TOC at the different stages of the photocatalytic reaction represented the degree of organic substrates mineralization by $AgIn_5S_8$. Table 1 showed the decay of TOC of MO solution. Under visible light irradiation for 15 h, the TOC values finally decreased to ca. 54.5% of the original MO solution. The reason for the incomplete mineralization might be due to some stable byproducts.

3.6. The stability of $AgIn_5S_8$ photocatalyst

In order to test the chemical stability of $AgIn_5S_8$ photocatalyst, XRD and XPS were carried out to test the crystal phase and surface state of $AgIn_5S_8$ photocatalyst before and after reaction. As shown in Fig. 8, the XRD patterns of the fresh and used samples were almost the same. This indicated that after a long time exposure to wet environment and irradiation of visible light, the crystal phase of $AgIn_5S_8$ did not change. The XPS analysis showed that only Ag, In, S, C, and O peaks could be observed in the survey spectrum (Fig. 9a). The small amount of C and O elements might come from the adsorbed gas molecular such as O_2 and CO_2. From the high resolution spectra of Ag3*d*, In3*d*, and S2*p* (Fig. 9b and c), no obvious peak shift was found in the used sample, indicating the valence of Ag, In and S did not change. This result illuminated that no photocorrosion or photodissolution was observed on the surface of $AgIn_5S_8$. In addition, we also tested the stability of photocatalytic activity of $AgIn_5S_8$. The $AgIn_5S_8$ photocatalyst was reused five times for the MO decomposition, as shown in Fig. 10. In every run of the lifetime test, $AgIn_5S_8$ did not exhibit obvious loss of activity, and the degradation rate in the five runs test only slightly changed. In conclusion, the stability of $AgIn_5S_8$ photocatalyst was proved by XRD, XPS, and lifetime test, making the application of $AgIn_5S_8$ photocatalyst in industry practical.

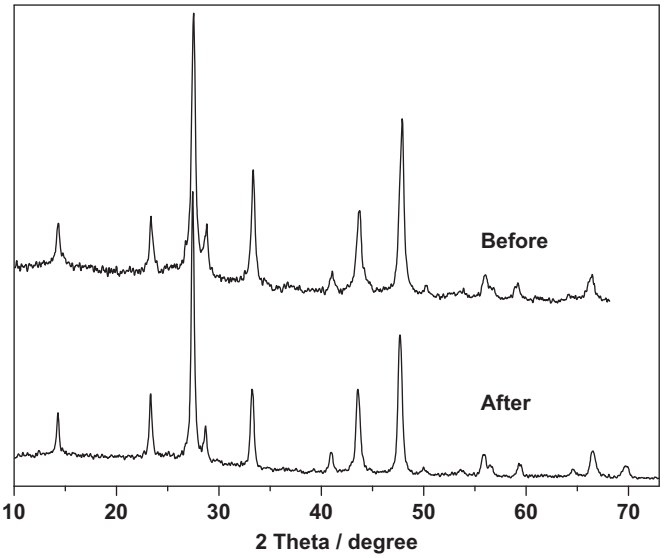

Fig. 8. The comparison of XRD patterns of $AgIn_5S_8$ before and after degradation.

3.7. Mechanism

The reactive active species such as hydroxyl radicals (•OH) and superoxide radicals ($O_2^{\bullet -}$) which possibly involved in the photodegradation process was examined by ESR technique. The experiments were carried out in the present of DMPO for in both water and methanol. Fig. 11 illustrated the ESR spectra of the DMPO-O_2^- spin adduct under ambient conditions in DMPO/$AgIn_5S_8$/methanol dispersion. The four stronger and obvious characteristic peaks of DMPO-O_2^- adducts can be observed in the methanol solvent. Fig. S3 showed the ESR spectra of the DMPO-·OH spin adduct in DMPO/$AgIn_5S_8$/H_2O dispersion. Four characteristic peaks of the DMPO-•OH adduct were observed after 300 s visible light illumination in the water solvent, however, the intensity was extremely weak according to the figure, indicating very small amount of •OH was produced in DMPO/$AgIn_5S_8$/H_2O system. The amount of •OH was so small that it has little effect. It is reasonable to conclude that O_2^- and very small amount of •OH were generated in the $AgIn_5S_8$ photocatalytic system under visible light irradiation.

The DPD method [18] was widely employed for the detection of H_2O_2. This method is based on the POD-catalyzed oxidation by H_2O_2 of DPD. The sequence of reaction leads to the formation of the radical cation, $DPD^{\bullet +}$, which forms a fairly stable color, with one absorption maxima at 510 nm and one at 551 nm. The procedure of DPD method was according to the literature. The result is shown in Fig. 12. Curve-a from Fig. 12 showed two absorption maxima, one at ca. 510 and the other at ca. 551 nm, indicating H_2O_2 was actually generated in $AgIn_5S_8$/H_2O (40 mg/80 mL) suspension after 30 min of visible light irradiation. While for the water sample (curve-b), there was no obvious peak observed under the same condition. So we therefore concluded that H_2O_2 was actually generated during the $AgIn_5S_8$ photocatalytic process.

Hole (h^+) was considered as an important active species in the photocatalytic system. We investigated the influence of holes on the photocatalytic activity of $AgIn_5S_8$. Photocatalytic decomposition of MO in an aqueous suspension of $AgIn_5S_8$ was examined in the presence of ammonium oxalate (AO), which was known as

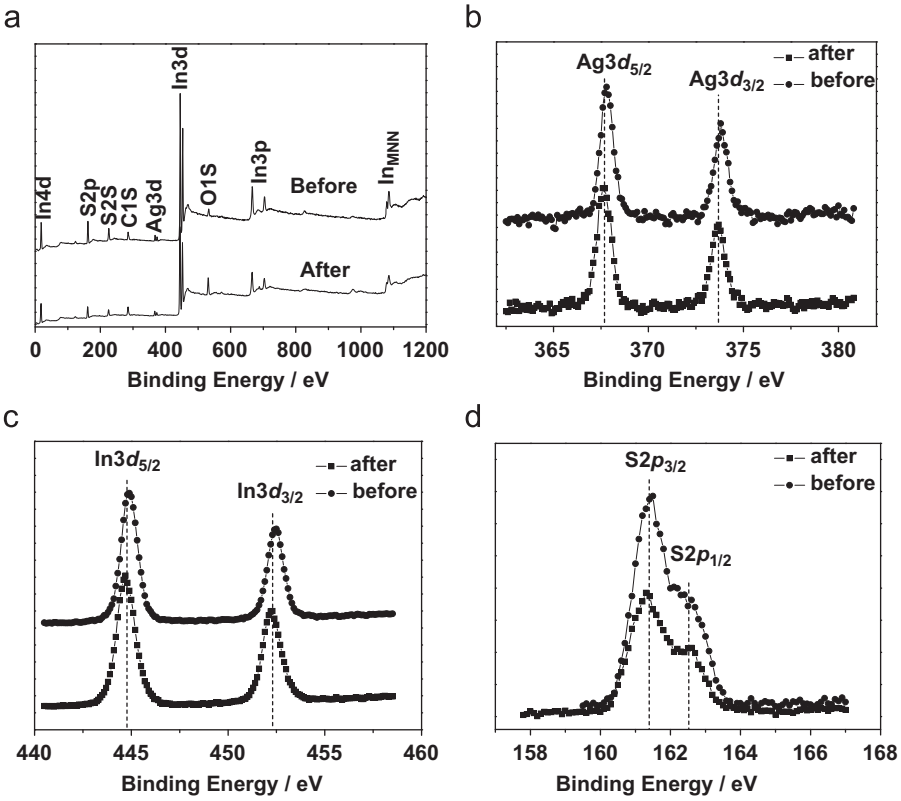

Fig. 9. The comparison of XPS spectra of $AgIn_5S_8$ before and after degradation: (a) survey; (b) Ag3*d*; (c) In3*d*; and (d) S2*p*.

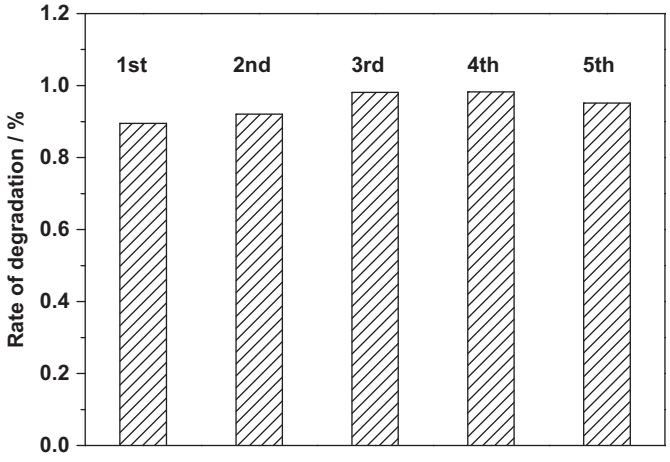

Fig. 10. The rate of degradation of cycling runs for the photodegradation of MO in the presence of $AgIn_5S_8$ under visible light irradiation.

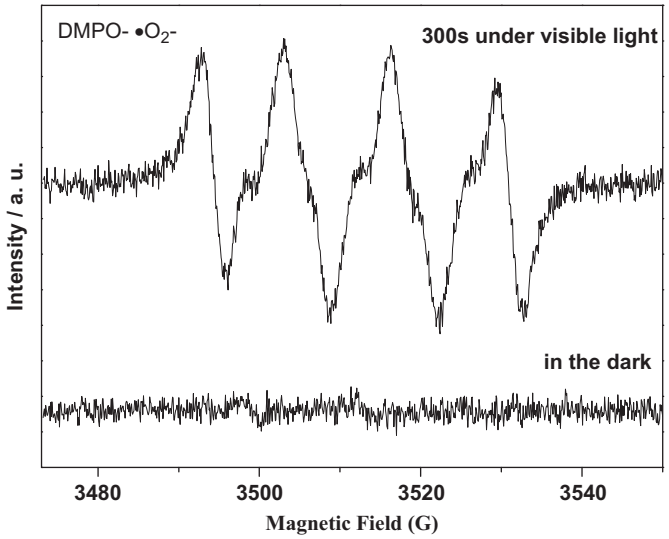

Fig. 11. DMPO spin-trapping ESR spectra of DMPO-O_2^- in $AgIn_5S_8$ photocatalytic system.

a hole scavenger [23]. Fig. 13 showed that the degradation rate was remarkably reduced after the addition of AO, indicating that holes in the $AgIn_5S_8$ photocatalytic system may oxidize the dye directly. To sum up, O_2^-, H_2O_2, and h^+ might be the mainly active species, which were responsible for the degradation of organic pollutants over $AgIn_5S_8$ photocatalyst.

The energy band structure of a semiconductor is the foundation of exploring its photocatalytic mechanism of azo dyes decomposition. The conduction band potential (E_{CB}) of n-type semiconductor is very close to (usually 0.1–0.2 V more negative) the V_{fb} [24]. Herein, we used an electrochemical method [25] to measure the V_{fb} of $AgIn_5S_8$ semiconductor particles. As seen in Fig. 14, the Mott–Schottky plot remained linear in the range of –0.25 and 0.5 V. The value of V_{fb} was about –1.36 V vs. SCE at pH=3 (equivalent to –1.36 V vs. NHE at pH=7). The Mott–Schottky plot also showed that the as-prepared $AgIn_5S_8$ sample had the nature of n-type semiconductor. So we inferred that the E_{CB} of $AgIn_5S_8$ was about –1.46 V. Because the band gap of $AgIn_5S_8$ sample was 2.57 eV from above discussion, the value band potential (E_{VB}) of $AgIn_5S_8$ was about 1.11 V.

Base on the experiment results, a possible mechanism for photocatalytic decomposition of organic pollutant over $AgIn_5S_8$ was proposed (Scheme 2 and Eq. 1–5). The process was listed as following: (a) Under visible light irradiation, some electrons were excited from valence band into conduction band, leading to the generation of electron–hole (e^-–h^+) pairs (Eq. (1)). (b) In the

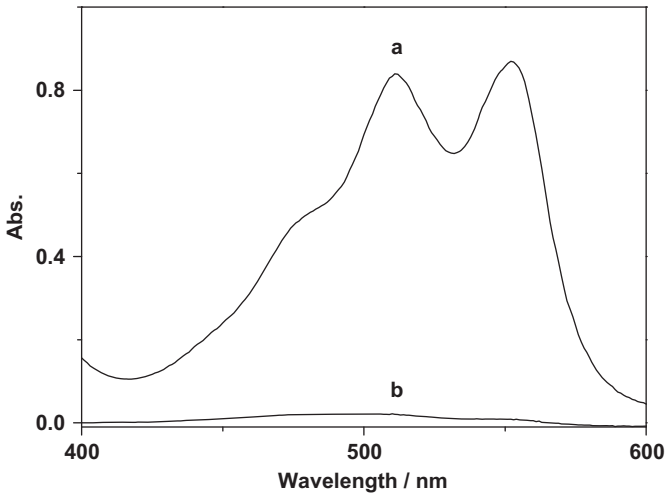

Fig. 12. Absorption spectra of the DPD/POD reagent after reaction with different sample: curve (a) was obtained by addition of DPD and POD to the degraded solution after 30 min of irradiation; curve (b) was obtained by addition of DPD and POD to the water sample.

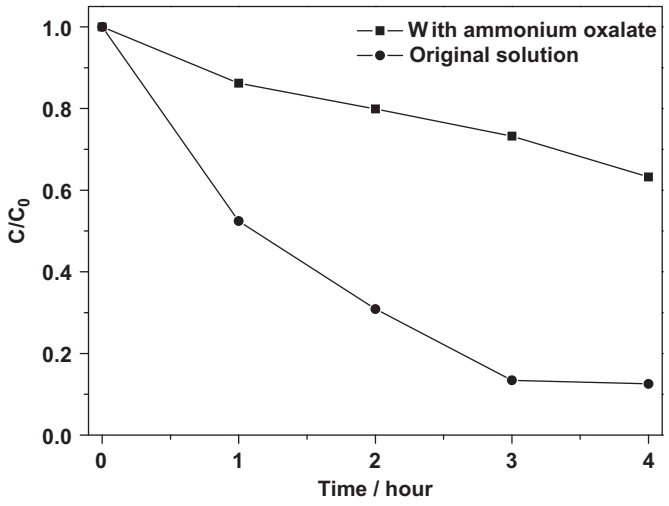

Fig. 13. Photocatalytic degradation of MO over $AgIn_5S_8$ powders in the presence of ammonium oxalate.

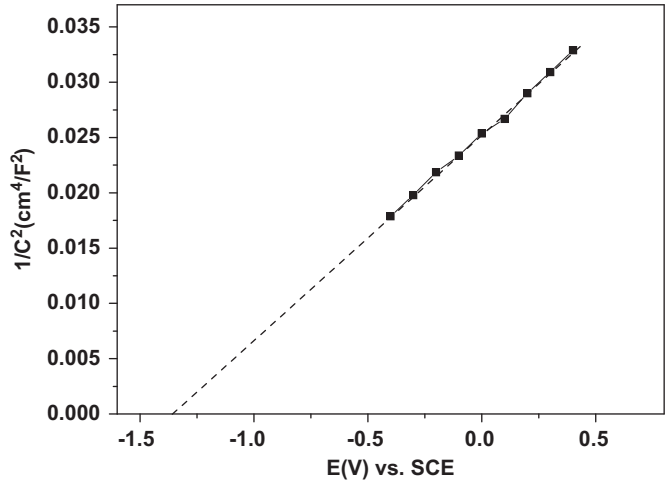

Fig. 14. The Mott–Schottky plot of $AgIn_5S_8$ electrode in 0.1 M $LiClO_4$ at pH 3.

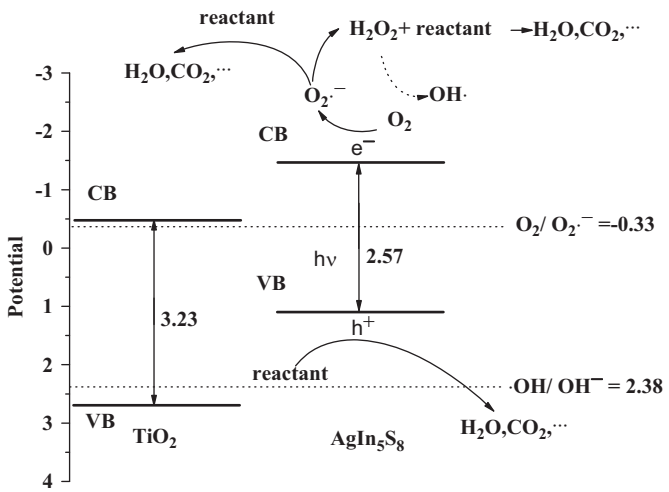

Scheme 2. Proposed mechanism for the visible light photocatalytic reaction of dye on $AgIn_5S_8$.

conduction band, some of the excited electrons recombined with holes. On the other hand, because the E_{CB} of $AgIn_5S_8$ (−1.46 V) was more negative than $E^{\circ}(O_2/O_2^{\cdot-})$ (−0.33 V vs. NHE)[26], the electrons transferred to the surface of catalyst could reduce O_2 to produce $O_2^{\cdot-}$ (Eq. (2)). (c) Under visible light irradiation, H_2O_2 could be generated through the combination of $O_2^{\cdot-}$ and H^+ (Eq. (3)). (d) On the other hand, because the E_{VB} of $AgIn_5S_8$ (1.11 V) was more negative than $E^{\circ}(\bullet OH/OH^-)$ (2.38 V vs. NHE) [26], the holes could not oxidize hydroxyl to produce •OH. So the only approach to produce a very small amount of ·OH might be through the reduction of H_2O_2 (Eq. (4)) rather than oxidation of hydroxyl. Herein, the holes directly oxidized the dye molecule absorbed on the surface of photocatalyst (Eq. (5)). These $O_2^{\cdot-}$, H_2O_2, and h^+ were responsible for the degradation of the dye (Eq. (5)). The reaction could be described as follows:

$$AgIn_5S_8 + h\nu \rightarrow AgIn_5S_8(e_{cb}^-) + AgIn_5S_8(h_{vb}^+) \quad (1)$$

$$AgIn_5S_8\ (e_{cb}^-) + O_2 \rightarrow AgIn_5S_8 + O_2^{\cdot-} \quad (2)$$

$$O_2^{\cdot-} + AgIn_5S_8\ (e_{cb}^-) + 2H^+ \rightarrow H_2O_2 \quad (3)$$

$$H_2O_2 + AgIn_5S_8\ (e_{cb}^-) \rightarrow \bullet OH\ (\text{a very small amount}) + OH^- \quad (4)$$

$O_2^{\cdot-}$ H_2O_2 or h_{vb}^++dyes→peroxylated or hydroxylated intermediates →→ degraded or mineralized products (5)

4. Conclusion

$AgIn_5S_8$ powder has been successfully synthesized using microwave hydrothermal method without any organic solvent, surfactant, or template. This method has been found to be highly efficient, effective and mild for scale-up industrial production of high-quality photocatalysts. The photocatalytic activity of $AgIn_5S_8$ was investigated by the decomposition of MO under visible light irradiation. Compared with $TiO_{2-x}N_x$ photocatalyst, $AgIn_5S_8$ exhibited a higher activity under the same condition. After 4 h of reaction time, the mineralization ratio of MO via $AgIn_5S_8$ photocatalyst was ca. 45.5%. Through the LCMS technology, we inferred the possible structures of decomposed products and degradation pathway of MO. The active species (such as $O_2^{\cdot-}$, H_2O_2, and h^+) responsible for the degradation of MO were

detected in the $AgIn_5S_8$ photocatalytic system. Base on the energy band structure and experiment results, a possible mechanism for the photocatalytic degradation of MO over $AgIn_5S_8$ was proposed. The stability of $AgIn_5S_8$ photocatalyst was proved, making the application of $AgIn_5S_8$ photocatalyst in industry practical.

Acknowledgments

This work was financially supported by the National Natural Science Foundation of China (20537010, 20677010, and 20873023). An "863" Project from the MOST of China (2006AA03Z340), National Basic Research Program of China (973 Program, 2007CB613306), and the Science Foundation of Fujian, China (2007F5066, JA07001, 0330-033064 and 0330-033070).

Appendix A. Supplementary materials

Supplementary data associated with this article can be found in the online version at doi:10.1016/j.jssc.2010.08.011.

References

[1] J.C. Zhao, T.X. Wu, K.Q. Wu, K. Oikawa, H. Hidaka, N. Serpone, Environ. Sci. Technol. 32 (1998) 2394–2400.
[2] O. Carp, C.L. Huisman, A. Reller, Prog. Solid State Chem. 32 (2004) 33–177.
[3] M.R. Hoffmann, S.T. Martin, W.Y. Choi, D.W. Bahnemann, Chem. Rev. 95 (1995) 69–96.
[4] S. Karvinen, R.J. Lamminmaki, Solid State Sci. 5 (2003) 1159–1166.
[5] T.X. Wu, G.M. Liu, J.C. Zhao, H. Hidaka, N. Serpone, J. Phys. Chem. B 103 (1999) 4862–4867.
[6] W.M. Du, X.F. Qian, J. Yin, Q. Gong, Chem. Eur. J. 13 (2007) 8840–8846.
[7] B.B. Kale, J.O. Baeg, S.M. Lee, H.J. Chang, S.J. Moon, C.W. Lee, Adv. Funct. Mater. 16 (2006) 1349–1354.
[8] J. Klaer, J. Bruns, R. Henninger, K. Seimer, R. Klenk, K. Ellmer, D. Braunig, Semicond. Sci. Technol. 13 (1998) 1456–1458.
[9] D. Chen, J.H. Ye, J. Phys. Chem. Solids 68 (2007) 2317–2320.
[10] Z.X. Chen, D.Z. Li, W.J. Zhang, Y. Shao, T.W. Chen, M. Sun, X.Z. Fu, J. Phys. Chem. C 113 (2009) 4433–4440.
[11] I. Konovalov, L. Makhova, R. Hesse, R. Szargan, Thin Solid Films 493 (2005) 282–287.
[12] I.V. Bodnar, V.F. Gremenok, Thin Solid Films 487 (2005) 31–34.
[13] A.F. Qasrawi, T.S. Kayed, I. Ercan, Mater. Sci. Eng. B 113 (2004) 73–78.
[14] K.W. Cheng, C.M. Huang, G.T. Pan, P.C. Chen, T.C. Lee, T.C.K. Yang, Mater. Chem. Phys. 108 (2008) 16–23.
[15] L.H. Lin, C.C. Wu, C.H. Lai, T.C. Lee, Chem. Mater. 20 (2008) 4475–4483.
[16] X.L. Hu, J.C. Yu, J.M. Gong, Q. Li, Cryst. Growth Des. 7 (2008) 2444–2448.
[17] X.F. Chen, X.C. Wang, Y.D. Hou, J.H. Huang, L. Wu, X.Z. Fu, J. Catal. 255 (2008) 59–67.
[18] H. Bader, V. Sturzenegger, J. Hoigne, Water Res. 22 (1988) 1109–1115.
[19] T.C. Deivaraj, J.H. Park, M. Afzaal, P. O'Brien, J.J. Vittal, Chem. Commun. (2001) 2304–2305.
[20] M.A. Butler, J. Appl. Phys. 48 (1977) 1914–1920.
[21] X. Mathew, P.J. Sebastian, Sol. Energy Mater. Sol. Cells 59 (1999) 85–89.
[22] H. Irie, Y. Watanabe, K. Hashimoto, J. Phys. Chem. B 107 (2003) 5483–5486.
[23] H. Kominami, A. Furusho, S. Murakami, H. Inoue, Y. Kera, B. Ohtani, Catal. Lett. 76 (2001) 31–34.
[24] S.R. Morrison, Electrochemistry at Semiconductor and Oxidized Metal Electrodes, Plenum Press, New York, 1980 (Chapter 4).
[25] R. Ramesham, Thin Solid Films 322 (1998) 158–166.
[26] Z.H. Li, T.T. Dong, Y.F. Zhang, L. Wu, J.Q. Li, X.X. Wang, X.Z. Fu, J. Phys. Chem. C 111 (2007) 4727–4733.